Theoretical Study on Mesoscopic-Size Impurity Effects in the Charge Separation Process of Organic Photocells

Journal:	*Physical Chemistry Chemical Physics*
Manuscript ID	CP-ART-12-2017-008125.R2
Article Type:	Paper
Date Submitted by the Author:	27-Apr-2018
Complete List of Authors:	Shimazaki, Tomomi; Kobe University, Graduate School of Science, Technology and Innovation; RIKEN, RIKEN-AICS Tashiro, Motomichi; Toyo University Nakajima, Takahito; RIKEN Advanced Institute for Computational Science,

Theoretical Study on Mesoscopic-Size Impurity Effects in the Charge Separation Process of Organic Photocells

Tomomi Shimazaki[1,2], Motomichi Tashiro[3], and Takahito Nakajima[2]

1, Kobe University, Graduate School of System Informatics
Rokkodai-cho 1-1, Nada-ku, Kobe 657-8501, Japan

2, RIKEN, Advanced Institute for Computational Science
Minatojima-minami-machi 7-1-26, Chuo-ku, Kobe, Hyogo 650-0047, Japan

3, Toyo University, Department of Applied Chemistry
Kujirai 2100, Kawagoe-shi, Saitama 350-8585, Japan

ABSTRACT

A bulk-heterojunction structure is often employed to develop high-performance organic photocells, in which the donor and acceptor regions are complexly intertwined. In such situations, the mesoscopic-scale islands and peninsulas that compose the donor materials may be formed in the acceptor region. Alternatively, the donor region may extend deeply into the acceptor region. This yields mesoscopic-size impurities in the charge separation (exciton dissociation) process of organic photocells and prevents the dissociation of excitons (electron–hole pairs). We previously reported on the effect of the cooperative behavior between the hot charge transfer (CT) state and the dimensional (entropy) effect on the charge separation process. In this paper, we discuss the mesoscopic-scale impurity effect on the charge separation process in PCBM acceptor models by considering the hot CT state and dimensional effects. In addition, we discuss atomic-scale effects such as molecular distortions and conformation changes using molecular dynamics (MD) simulations.

1. Introduction

Organic photocells can possess various features that differ from those of silicon-based solar cell devices. For example, it is expected to develop flexible and lightweight solar cells with high power conversion efficiencies by utilizing the characteristics of organic materials. To create such devices, we need to comprehensively understand the photocurrent generation mechanism in organic solar cells. Photocurrent generation can be divided into four processes: photon absorption (exciton generation), exciton diffusion, charge transfer, and charge separation. In this paper, we focus on the charge separation (exciton dissociation) process, where the strongly bound electron–hole pair (exciton) is completely dissociated to form free carriers.[1] This phenomenon occurs around the donor–acceptor interface of organic photocells. Several mechanisms have been proposed to explain the exciton dissociations related to the strong interactions between electrons and holes.[2-10] For example, in the hot mechanism, a hot electron with excess energy is injected into the acceptor region at the beginning of the charge separation process.[1, 11-20] The lowest unoccupied molecular orbital (LUMO) energies of donor and accepter molecules are usually different; therefore, the band offset in the conduction band exists at the donor–acceptor interface. The band offset provides excess energy to the electron transferred from the donor to the acceptor region. This energetically high state is termed the hot charge transfer (CT) state. The excess energy is rapidly dissipated, and the hot CT state eventually becomes an energetically stable (relaxed) state. However, in the hot mechanism, the excess energy of the hot CT state is considered necessary to undo the strong interactions between the electron and the hole. Shen et al. estimated exciton dissociation and charge recombination rates by using density functional theory (DFT), to investigate the hot CT state effect in the charge separation

process.[21] Gautam et al. described behaviors of high-energy states in polymer/fullerene blends by using a population dynamic simulation.[22] Fazzi studied excited state evolutions at the P3HT/PCBM interface through a bottom-up approach with first-principle calculations.[23] Sosorev et al. employed an analytical kinetic model to handle two-step charge generation through hot CT states.[24] On the other hand, we previously discussed a theoretical methodology for the hot exciton dissociation process and noted the importance of the cooperative behavior between the hot CT state and the dimensional (entropy) effect.[25-28] However, other factors can also have a strong influence on exciton dissociations in organic photocells. In particular, mesoscopic-scale impurities strongly disturb electron diffusion in the acceptor region of an organic photocell. This paper discusses the mesoscopic-scale impurity effect by considering the hot CT state and the dimensional effect.

Various types of polymer material are used for the donor region in organic photocells. Conversely, fullerene derivatives such as PCBM are frequently adopted for use as the acceptor region. Recently, many organic photocell devices with high power conversion efficiencies have incorporated a bulk-heterojunction (BHJ) structure, in which the donor and acceptor materials are intertwined to overcome the short lifetime of the exciton.[29-32] Therefore, the donor–acceptor interface usually has a complex structure. In some circumstances, donor polymer materials may extend significantly into the PCBM acceptor region. In other cases, islands and peninsulas, which are composed of polymers, may be created in the acceptor region. Indeed, recent theoretical and experimental studies have observed such complex BHJ structures and morphologies.[33-35] These complex BHJ structures may behave like impurities and obstacles in the exciton dissociation process. In particular, if the size of such impurities becomes mesoscopic in

scale, the impurities cannot be ignored. Therefore, this paper focuses on mesoscopic-scale effects on the exciton dissociation process. To quantitatively investigate the impurity effect, we calculate the exciton dissociation probability (efficiency). In the next section, we briefly explain our calculation methods. Results and discussion are presented in Section 3, and concluding remarks are given in Section 4.

2. Methods

2.1. Exciton dissociation probability

This section briefly explains the exciton dissociation process based on the 1D acceptor model.[25] The 2D and 3D cases can be readily obtained on the basis of the 1D approach.[26, 28] To consider the charge separation process with the hot CT state effect, we employ an n-hopping sites model with relaxed and hot states.[25] A hot electron with excess energy corresponding to the band offset E_{offset} is injected into the hot state of the first site. However, the population of the hot electron decreases at a rate of t_h^{-1} via energy dissipation processes. As such, the injected electron randomly moves between the sites, losing the excess energy. Electron–hole recombination occurs only at the first site. We set a sink site next to the n-th site, where the binding energy between an electron and a hole is equivalent to the thermal energy. An electron that can reach the sink site is regarded as a free carrier. For electron transition between sites, we assume the following Miller–Abrahams transition rate[25, 26, 36-39]:

$$a_{i\to j}^{r} = a_c \exp\left(-\frac{E_j - E_i + \left|E_j - E_i\right|}{2k_B T}\right) \quad (1\text{-}1)$$

$$a^{h}_{i\to j} = a_c \exp\left(-\frac{E_j - E_i + \left|E_j - E_i\right|}{2(E_{offset} + k_B T)}\right), \tag{1-2}$$

where $a^{r}_{i\to j}$ and $a^{h}_{i\to j}$ are the transition rates from site i to site j for the relaxed and hot states, respectively. k_B is the Boltzmann constant, and T is temperature. The constant a_c is related to the coherent transition (tunneling) rate. In our calculations, the a_c parameter strongly depends on the site positions, which are sampled from molecular dynamics (MD) simulations; these details will be discussed later. $E_{i(j)}$ is the energy of site $i(j)$. This paper does not assume the external electric field but instead focuses on the hot CT effect; as such, the following Coulomb interaction, with the dielectric constant ε_s, is employed to describe the energy level:

$$E_i = -\frac{1}{4\pi\varepsilon_0\varepsilon_s}\frac{e^2}{\left|\mathbf{R}_i\right|}, \tag{2}$$

where ε_0 is the vacuum permittivity, $\mathbf{R}_i$ denotes the distance between site i and a hole, and e is the elementary charge. Then, we can obtain the exciton dissociation probability h as follows:

$$\eta = \eta^h - \sum_{s=1}^{n} \frac{1+\tau_0^{-1}\sum_{j=1}^{s-1}\frac{1}{a^r_{j\to j+1}}\exp\left(\frac{E_j - E_1}{k_B T}\right)}{1+\tau_0^{-1}\sum_{j=1}^{n}\frac{1}{a^r_{j\to j+1}}\exp\left(\frac{E_j - E_1}{k_B T}\right)} \frac{\left[\mathbf{B}_h^{-1}\right]_{s1}}{\tau_h} \tag{3-1}$$

$$\eta^h = -a^h_{n\to \mathrm{sink}}\left[\mathbf{B}_h^{-1}\right]_{n1}, \tag{3-2}$$

where t_0^{-1} is the rate for electron–hole recombination and h^h represents the contribution of the hot states to the efficiency. The $\mathbf{B}_h$ matrix can be determined from

the rate equations; its explicit expression is discussed in our previous studies.[25, 26] Here, we should emphasize that Eq. (3-1) reduces to the Onsager and Frenkel models in some limiting cases.[25, 26, 40-45]

2.2. Molecular dynamics simulations

MD simulations have been performed to estimate the structure of the PCBM layer. The OPLS all-atom force field parameters,[46] along with additional parameters,[47] were used to evaluate forces and energies. The initial structures of the columnar 1D, plate-shaped 2D, and bulk 3D PCBM accepter models were constructed based on an experimental crystal structure.[48] The 1D model contains 320 PCBM molecules extending 35,270, and 30 Å in the x-, y-, and z-directions, respectively. The 2D model contains 5,120 PCBM molecules extending 505,270, and 30 Å in the x-, y-, and z-directions, respectively. The bulk 3D model contains 16,200 PCBM molecules in a box with dimensions of 250, 300, and 250 Å in the x-, y-, and z-directions, respectively. After construction of the initial structure, the system was equilibrated for 0.5 ns at a constant temperature of 298 K and pressure of 1 atm under periodic boundary conditions. To obtain an amorphous-like structure, the system was heated to 800 K for 0.5 ns and then annealed down to 298 K in 0.5 ns. In order to sample atomic-scale conformation changes of the PCBM molecules in the bulk 3D model, the MD simulation was performed for 5 ns, with snapshots of the structure taken every 2 ps. The velocity-Verlet method, with a time step of 1 fs, was used for time integration. All MD simulations were performed with the Lammps program package.[49, 50] We employed the PCBM models described above for calculations of the exciton dissociation probability in the charge separation process. Additionally, we periodically extended the above

model in the x- and z-directions for the 3D cases. In this paper, each PCBM molecule functions as a site for electron-hopping models.

3. Results and discussions

3.1. Exciton dissociations for PCBM acceptor models

This section presents the exciton dissociation probability for columnar- and plate-shaped acceptor models composed of PCBM molecules, as shown in Figures 1a and 1b, where, respectively, an injected electron is shown to move randomly in (quasi) 1D and 2D ways. The bulk acceptor model is also used to study 3D random motion. In the BHJ structure of an organic photocell, exciton diffusion may be restricted by protruding donor regions or large impurities. The columnar- and plate-shaped acceptor models are useful for investigating fundamental behaviors when random electron motion is restricted. We calculated the exciton dissociation probabilities for these models by changing the band offset at the donor–acceptor interface. We summarize these calculation results in Figure 1c. Here we set an initial separation distance of 8.5 Å for the electron–hole pair. We use a cutoff distance (Onsager radius) of 200 Å to set the sink sites, which is sufficient to thermally separate electron–hole pairs in organic semiconductors with a dielectric constant of $\varepsilon_s = 4.0$ at room temperature ($T = 300$ K). We obtain the a_c parameter in Eq. (1) from the following equation.

$$a_c = a_0 \exp(-\ (\left|\mathbf{R}_i - \mathbf{R}_j\right| - R_0)/s\ ), \tag{4}$$

where $\mathbf{R}_i$ and $\mathbf{R}_j$ represent the positions of i-th and j-th PCBM molecular sites, respectively. We use $R_0 = 10$ Å, which is the typical distance between the nearest sites

in the crystal structures of fullerene derivatives.[51] We also use $a_0^{-1} = 10$ fs and $s = 2.0$ Å, which are typically used to express PCBM models.[26, 51] In this paper, we extract the positions of PCBM molecules from MD trajectories, and therefore various distances between site locations are included in our calculation models. The a_c parameter strongly depends on those distances as seen in equation (4), and therefore transition rates have strong dependency on the site positions. For example, the transition rate exponentially decreases when the distance between sites becomes large.

Exciton recombination times of about 50 ps to 1 ns are observed experimentally; therefore, we set $\tau_0 = 100$ ps.[1, 52] The lifetime of hot CT states ranges from 1.0 to 3.0 ps[19, 53-55]; therefore, we employ $t_h = 2.0$ ps in this paper. These parameter values are used for the calculations in the following sections.

From Figure 1c, we observe that the columnar-shaped PCBM acceptor model gives the lowest exciton dissociation probabilities in all band offsets. Conversely, the bulk PCBM model presents the highest probabilities, and the plate-shaped model yields the second highest probabilities. Compared with other models, the exciton dissociation probability of the bulk PCBM model is quickly saturated, even in the lowest band offset region. In other words, the bulk 3D acceptor model can more easily maintain the performance of organic photocell devices, even in the relatively low band offset cases. The low band offset is required to realize large open-circuit voltages in organic photocell devices and is an essential factor for the development of efficient devices.[28, 56] In the columnar- and plate-shaped models, electron movement is restricted to quasi 1D and 2D spaces; therefore, the exciton dissociations are suppressed even in high band offset cases. Conversely, the bulk 3D PCBM acceptor model shows superior

performance for low band offsets. Thus, the dimensional (entropy) effect yields a strong impact on the exciton dissociation process. On the other hand, in small band offset cases, the exciton dissociation probability became low, even in the bulk 3D model. The cooperative behavior between the hot CT state and the dimensional effect is essential in realizing efficient exciton dissociations.[26, 28]

3.2. Mesoscopic-scale impurities in plate-shaped PCBM acceptor models

Next, we discuss the effects of mesoscopic-scale impurities, which disturb the diffusion of electrons injected into the 2D plate-shaped acceptor model. The 3D bulk case will be discussed later. The BHJ structures of organic photocells are complex, and various types of impurity can exist in the acceptor region. Therefore, it is clearly beyond the scope of the present work to consider all types of impurity. Instead, this paper focuses on simplified impurity models and investigates their fundamental behavior in relation to the charge separation process. For this purpose, we adopted the rectangular-shape impurities depicted in Figure 2a. We assume that a rectangular-shape impurity extends infinitely in the direction perpendicular to the page (z-axis) and that the electron cannot pass through the impurity. To move to the other side of the impurity, the electron must bypass the impurity along the x-axis. In this paper, we examine several mesoscopic-scale impurities of differing widths. In addition, we alter the distance between the mesoscopic-scale impurities and the hole. Figures 2b and 2c show the exciton dissociation probabilities of models having rectangular-shape impurities with widths of 100 and 300 Å, respectively. In each figure, dash, dash–dot, and dash–dot–dot lines indicate models with an impurity located 50, 100, and 150 Å, respectively, away from the hole position. For comparison, we also present calculation results for

cases without impurities (black solid lines). From these calculations, we can confirm that the mesoscopic-scale impurities can have a strong impact on the charge separation process, and in some cases, they markedly reduce the exciton dissociation probability, as shown in Figure 2c. For example, when the model with a width of 300 Å is located at a distance of 50 Å from the donor–acceptor interface, an exciton dissociation probability of 0.38 is obtained for the 0.3 eV band offset case. In the absence of the impurity, a probability of 0.67 is calculated. When a mesoscopic-scale impurity is located 100 or 150 Å away from the interface, the exciton dissociation probabilities become 0.47 and 0.52, respectively. Conversely, Figure 2b shows that small impurities do not strongly affect the exciton dissociation process. For example, even if an impurity with a width of 100 Å is located 100 Å from the hole position, a high exciton dissociation probability of 0.64 is obtained at the band offset of 0.3 eV. Thus, closer and larger mesoscopic-scale impurities more strongly disturb the exciton dissociations. However, note that the impurity effect becomes very small when the impurity is smaller than about 100 Å.

3.3. Mesoscopic-scale impurities in 3D acceptor models

In this section, we discuss the exciton dissociation process for 3D acceptor models. We show calculation results focusing on the mesoscopic-scale impurity effect in Figure 3. Here, the same parameters used in the previous section are employed to obtain the calculation results. In the 3D models, we employ rectangular-shape impurity models similar to those used in the previous section. The rectangular-shape impurities extend infinitely in the z-axis direction. Electrons injected into the acceptor region must bypass the rectangular-shape impurity. In the bulk model case, electrons can move randomly in

three dimensions if no impurities exist. Conversely, electron diffusion is limited to (quasi) 2D random movements when a mesoscopic-scale impurity extending infinitely in the z-axis direction needs to be bypassed. In the 2D acceptor model case, the electron diffusion is (quasi) 1D when avoiding a mesoscopic-scale impurity. We examined mesoscopic-scale impurities of 100 and 300 Å widths, and we summarize the exciton dissociation probabilities relating to these impurities in Figures 3a and 3b, respectively. We also change the position of the impurity models, with distances of 50, 100, and 150 Å used; these calculation results are represented by the dash, dash–dot, and dash–dot–dot lines, respectively. In addition, for comparison, we depict the dissociation probabilities in the absence of impurities (solid line). These calculation results show that the exciton dissociation probability decreases when the width of the rectangular-shape impurity becomes large. For example, in the 100 Å width case, a dissociation probability of 0.82 is calculated at the band offset of 0.3 eV when the mesoscopic-scale impurity is located at a distance of 50 Å from the donor–acceptor interface. In the 300 Å case, an exciton dissociation probability of 0.68 is obtained. The position of the mesoscopic-scale impurity also has a strong influence on the exciton dissociation process. When an impurity with a width of 300 Å is located at a distance of 50 Å from the hole position, an exciton dissociation probability of 0.66 is calculated at the band offset of 0.2 eV. In the 100 and 150 Å distance cases, probability values of 0.74 and 0.80 are obtained, respectively. Thus, when a larger mesoscopic-scale impurity is located closer to the donor–acceptor interface, it more strongly disturbs the exciton dissociations. In addition, Figure 3a suggests that impurities with sizes smaller than 100 Å have only a low impact on the exciton dissociation process. This tendency can also be observed in the plate-shaped 2D cases. The impurity effect becomes milder in the 3D

acceptor model, as confirmed by comparisons of Figure 2c and Figure 3b. In the plate-shaped acceptor model, an electron must bypass the impurity in a (quasi) 1D manner. Conversely, in the bulk model, an electron can avoid the impurity in a (quasi) 2D manner. In other words, there are more routes via which to bypass the impurity in the 3D model. This means that organic photocells having a higher dimensionality in the acceptor region may possess a stronger tolerance against mesoscopic-scale impurities, which helps in maintaining device performance.

3.4. Atomic- and mesoscopic-scale effects

In this section, we discuss the effects of atomic-scale conformation changes to PCBM sites. To consider these atomic-scale effects, we employ MD simulation, the computational details of which are described in Section 2.2. Each 2.0 ps MD snapshot is used to determine the structures of PCBM molecules in the 3D acceptor model. Then, the exciton dissociation probabilities are calculated based on these snapshots. In Figure 4, we summarize the calculation results, where the horizontal and vertical axes represent the snapshots and probabilities, respectively. Figures 4a and 4b show the exciton dissociation probabilities when band offsets of 0.1 and 0.3 eV are used, respectively. We calculated the averages and standard deviations (SD) of the fluctuating dissociation probabilities in the MD simulations. When a band offset of 0.1 eV is employed, average and SD values of 0.80 and 0.0015 are obtained, respectively. These values become 0.85 and 0.0010, respectively, in the 0.3 eV band offset case. These data show that the charge separation process is not a static phenomenon and that exciton dissociation probabilities vary according to the atomic-scale coordinates of the PCBM molecules.

Next, we discuss both atomic- and mesoscopic-scale effects. For this purpose, we

calculate exciton dissociation probabilities using the snapshot PCBM structures together with the mesoscopic-scale impurities. Figure 5 presents fluctuations in the exciton dissociation probabilities for these models. Band offset values of 0.1 and 0.3 eV are used to obtain Figures 5a and 5b, respectively. In these calculations, rectangular-shape impurities are set 50 Å away from the hole position. We examined impurities with widths of 100, 200, and 300 Å, which are depicted using green, blue, and red lines in Figure 5, respectively. For comparison, we also depict the calculation results for the case without mesoscopic-scale impurities (black solid lines). The highest dissociation probabilities are obtained for the case without impurities. Conversely, the mesoscopic-scale impurities yield strong reductions in the exciton dissociation probability. The atomic-scale effects are represented as fluctuations in the exciton dissociation probability. From Figure 5, we can clearly compare atomic-scale and mesoscopic-scale influences on the charge separation process. The reductions in the exciton dissociation probability due to mesoscopic-size impurities are much larger than the fluctuations induced by the atomic-scale distortions. These results suggest that mesoscopic-scale structures are essential to improving the performance of organic photocells.

In order to understand the effect of the acceptor and impurity arrangement on the charge separation process, we employed simplified geometries for the PCBM acceptor regions and the intervening impurities. In realistic BHJ organic solar cells, the acceptor region may have various dimensionalities and length scales depending on how they are manufactured, e.g., use of different solvents, processing additives, and annealing conditions.[57, 58] Such realistic BHJ morphologies can be generated by the Ising model,[59] numerical equations like the Cahn–Hilliard model,[60] or coarse-grained MD

simulations.[34, 61, 62] In many cases, these methodologies can take into account the effect of different processing conditions (different solvents, annealing conditions, etc).[34, 60-62] On the basis of these BHJ geometries, drift-diffusion, master-equation, or kinetic Monte Carlo studies have been performed to estimate device properties.[33, 63] It would be interesting to extend our model to realistic BHJ conditions, where the effect of complex morphologies could be examined.

3.5 discussions and comparisons with previous studies

Recent experimental and theoretical studies clearly showed that the BHJ structure can have complicated shapes of a few tens of nanometers in size.[33-35] Some of those can play as mesoscopic-size impurities. On the other hand, we examined impurities of 10-30 nm size in this work, and thus our simulation will be useful to understand the charge separation process in realistic BHJ conditions. Conversely, we showed that the influence of impurities 10 nm or less in size is small. This suggests that small differences on the BHJ structure are not so important on exciton dissociations.

In our calculation models, we assumed that the dielectric constants of donor and acceptor materials are the same for simplicity, because donor materials used in organic photocell have close dielectric constants to that of the PCBM acceptor region. The difference on the dielectric constants may affect site energies and transition rates. Conversely, in this study, we considered the influence of changes of transition rates induced by atomic-scale site distortions. The atomic-scale distortions exponentially affect transition rates. However, the atomic-scale effect on the exciton dissociation probability is much smaller compared with the mesoscopic-scale impurity effect.

Here, we discuss the exciton dissociation time. The main topic of this paper is to

investigate the influence of mesoscopic-size impurities together with the hot CT state and dimensional effects on the charge separation process. Therefore, we employed a time-independent and deterministic approach to calculate exciton dissociation probabilities, and thus it is difficult to directly discuss the exciton dissociation time. However, our researches suggest that exciton dissociations can quickly occur. We previously showed that the hot CT state is essential to separate geminate electron–hole pairs.[25, 26, 28] This also means that exciton dissociations hardly occur if the hot state falls into the relaxed state through the dissipation of the excess energy. In our calculations, the lifetime of several picoseconds have been also employed for the hot CT state.[25, 26, 28] Jailaubekov et al. experimentally reported the fast hot CT state cooling process and efficient charge separation.[19] These results indicate that the charge separation can occur within at least a few picoseconds, if hot CT states are involved in exciton dissociations. On the other hand, this paper assumes that only one electron-hole pair is involved in the exciton dissociation process for simplicity. In actual organic photocell, the charge separation process may proceed among multiple electrons and holes. To consider multiple electrons and holes, we may need to employ time-dependent simulation techniques. These time-dependent features will become important to understand the complex exciton dissociation process.

Finally, we comment on the cool and hot mechanisms for the charge separation process. At present, there have been several studies discussing cool mechanisms. In this paper, we took into account the hot CT state effect. On the other hand, the dimensional (entropy) and mesoscopic-size impurity effects discussed in this paper may be categorized into the cool mechanism. Thus, this paper shows the importance of cooperative behaviors between hot and cool mechanisms. However, we did not cover all

cool mechanisms. For example, Burke et al. discussed the role of the mixed region based on the Kinetic Monte Carlo simulation technique.[64] Wu showed that the inherent driving force formed by a stack of curved oligothiophene chains can assist to separate electron–hole pairs by using first-principles calculations.[65] Baranovskii et al. estimated exciton dissociation probabilities with dark-dipole, external electric fields, delocalization of hole, and dark-dipole.[10, 66] Some of these may be integrated into our simulation technique. Such studies will be useful to uncover complex behaviors on the charge separation process.

4. Concluding remarks

In this paper, we have discussed the charge separation process in the PCBM acceptor model of organic photocells, for which the exciton dissociation probabilities for columnar-, plate-, and bulk-shaped acceptor models were calculated. In particular, this paper focused on the mesoscopic-scale impurity effect. From these calculations, we can confirm that mesoscopic-scale impurities have a strong influence on the exciton dissociation process. When a larger mesoscopic-scale impurity is located close to the donor–acceptor interface, the exciton dissociation probability markedly decreases. However, in both plate- and bulk-shaped PCBM models, the impurity effect becomes very small when the width of a rectangular-shape impurity is 100 Å. This suggests that, when the size of an impurity is less than 100 Å, the impurity effect is negligible in relation to the charge separation process. We also found that these influences are stronger in the 2D acceptor model than they are in the 3D acceptor model. In the 2D case, an electron injected into the acceptor region needs to bypass an impurity in a (quasi) 1D manner. Conversely, in the 3D case, an electron can avoid an impurity in a

(quasi) 2D manner. Therefore, the dimensionality of the acceptor region plays an important role in determining tolerances relating to mesoscopic-scale impurities. We also discussed the atomic-scale effect on the charge separation process and showed the exciton dissociation probabilities using snapshots of MD simulations. These calculations showed that the probabilities fluctuate according to atomic-scale conformation changes of the PCBM molecules. However, the influences from these atomic-scale fluctuations are not strong compared with the mesoscopic-scale impurity effect.

The 3D bulk model showed a stronger tolerance to mesoscopic-scale impurities; as such, the control of the dimensionality of the acceptor region becomes important in developing efficient organic photocell devices. In addition, several studies have reported the importance of the mesoscopic-scale structures, conformations, and morphologies of donor and acceptor materials, each of which can strongly impact the performance of organic photocells.[1, 7, 55, 67-70] Therefore, the control of mesoscopic-scale conformations and morphologies is one of the key factors for fabricating high-efficiency organic photocells. Multilayer structures may be suitable in controlling these aspects[71]; however, we should also pay further attention to the various mesoscopic-scale effects. This paper focused on the fundamental effects of mesoscopic-scale impurities on the charge separation process; we therefore employed rectangular-shape impurities. However, our methodology can also handle more realistic conformations and structures around the donor–acceptor interface. Such simulations will be conducted to better understand the photocurrent generation mechanism in organic photocell devices.

Acknowledgments

This work was partially supported by the JSPS KAKENHI(15K05403, 16H00939), and the research project using K computer (hp160235), competitive funding for team-based basic researches of "Creation of Innovative Functions of Intelligent Materials on the Basis of the Element Strategy" from CREST, and FOCUS Establishing Supercomputing Center of Excellence. The computations were partially performed using Research Center for Computational Science, Okazaki, Japan.

Figure Captions.

Figure 1. Schematic figures of a) quasi-1D columnar-shaped and b) quasi-2D plate-shaped models, which are composed of PCBM molecules. c) Exciton dissociation probabilities in accordance with the band offset at the donor–acceptor interface. We also show calculation results from the 3D bulk-shaped PCBM acceptor model. Here, the horizontal axis is used for the band offset [eV] at the donor–acceptor interface, and the vertical axis indicates the exciton dissociation probability.

Figure 2. a) Schematic of the mesoscopic-scale impurity model. The rectangular-shape impurity disturbs the diffusion of electrons in the acceptor region. Electrons must bypass the impurity to escape from the hole. We calculate the exciton dissociation probability by changing the width of rectangular-shape impurities in the plate-shaped (2D) acceptor model: b) 100 and c) 300 Å. In addition, we modify the location of the mesoscopic-scale impurity. The dash, dash–dot, and dash–dot–dot lines indicate impurities located at 50, 100, and 150 Å from the hole position. For comparison, we also show calculation results for the case without an impurity, which are depicted by a black solid line in each figure.

Figure 3. Changes in exciton dissociation probability according to the width of the rectangular-shape impurities in the 3D acceptor model. We calculated exciton dissociation probabilities when the width of the rectangular-shape impurity was altered.

This paper examined a) 100 and b) 300 Å widths. We also changed the distance between the impurity and the hole; the dash, dash–dot, and dash–dot–dot lines indicate distances of 50, 100, and 150 Å. For comparison, we also show the calculation results for the case without an impurity, which are depicted by a black solid line in each figure.

Figure 4. Changes in exciton dissociation probability according to the trajectories of MD simulations in the bulk PCBM model. The probabilities are calculated for every 2-ps snapshot of the MD trajectory. Figures a) and b) show calculation results for band offsets of 0.1 and 0.3 eV, respectively. These calculations show that exciton dissociations vary in accordance with atomic-scale confirmation changes of the PCBM molecules.

Figure 5. Changes in exciton dissociation probability according to the trajectories of MD simulations. Here, we also consider the mesoscopic-scale impurity effect. Figures a) and b) present the calculation results for band offsets of 0.1 and 0.3 eV, respectively. To obtain these calculations, rectangular-shape impurities were located 50 Å away from the hole position. The green, blue, and red lines indicate impurity widths of 100, 200, and 300 Å. For comparison, we also depict calculation results for the case without an impurity, which are shown as a black solid line in each figure. When any impurity is not present, the highest exciton dissociation probabilities are obtained at each time step. The atomic-scale effect appears in the small fluctuations of the exciton dissociation probabilities. Conversely, mesoscopic-scale impurities greatly reduce the exciton dissociation probabilities. These calculations suggest that the mesoscopic-scale effects have a much larger impact on the charge separation process.

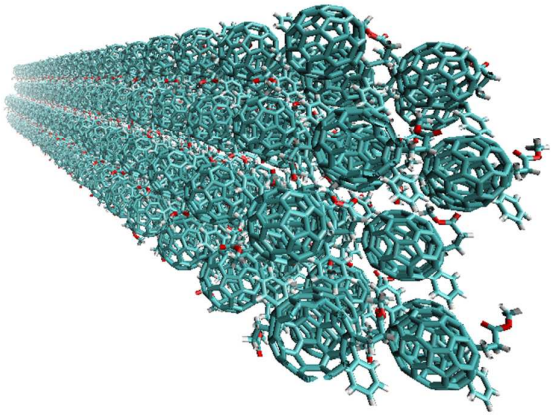

Figure 1a. T. Shimazaki et al.

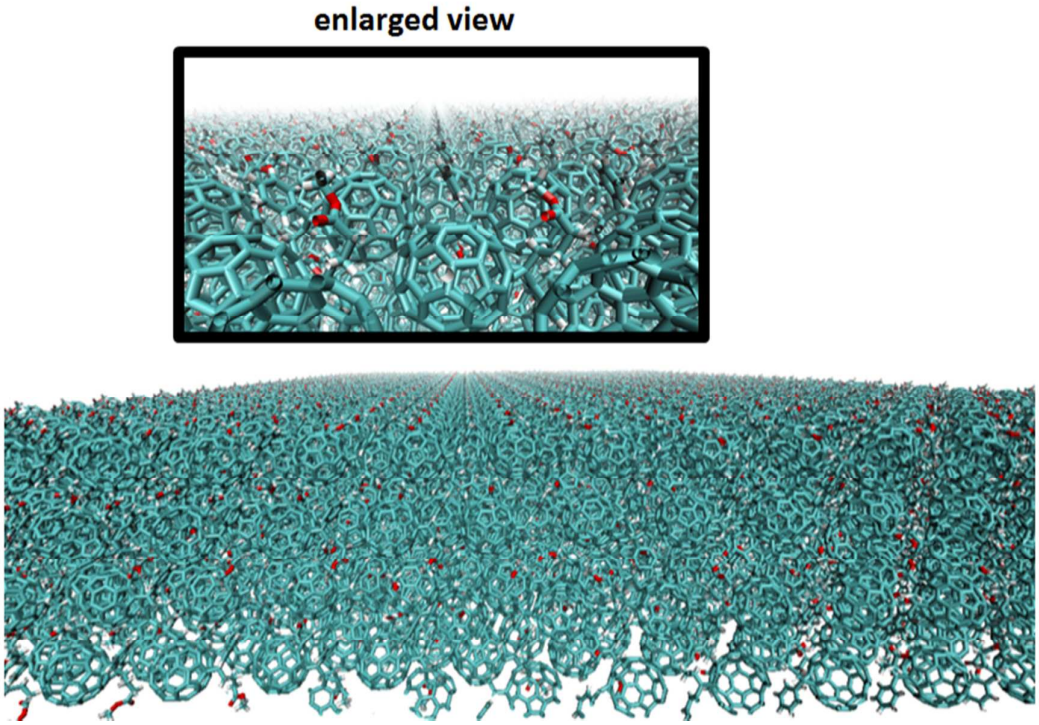

Figure 1b. T. Shimazaki et al.

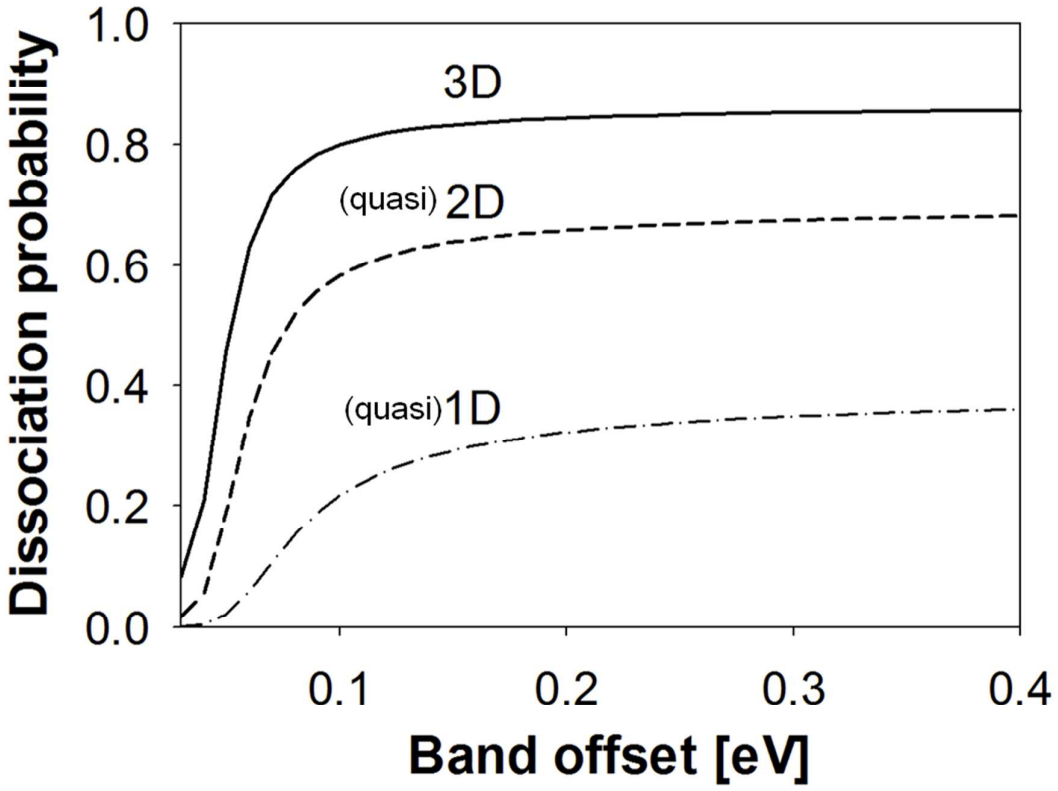

Figure 1c. T. Shimazaki et al.

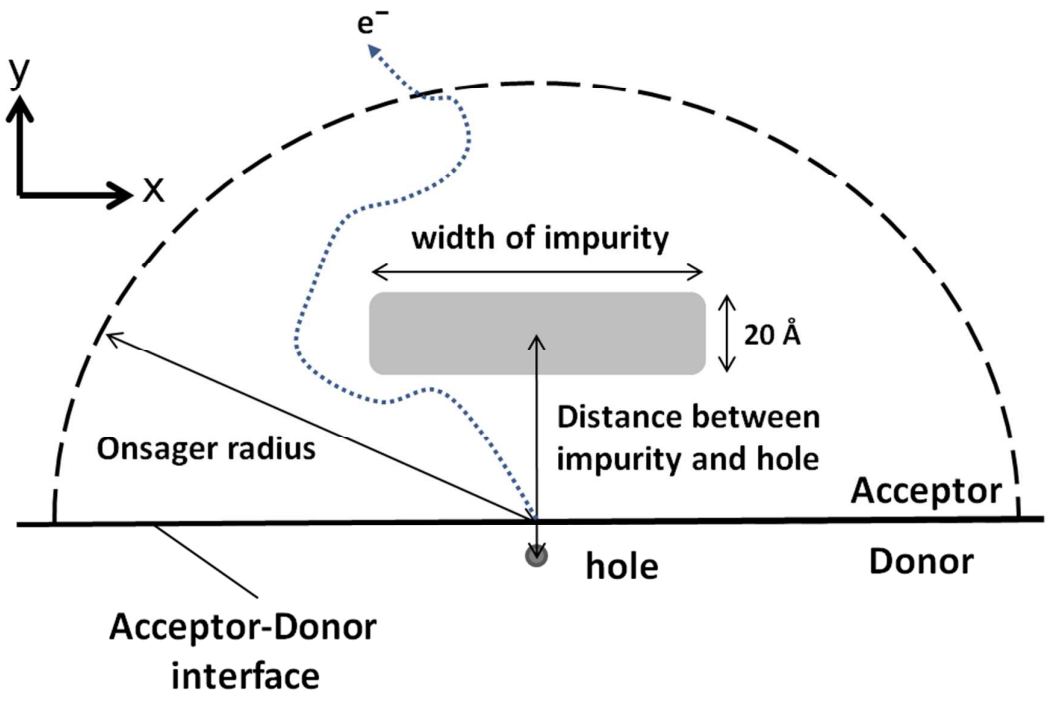

Figure 2a. T. Shimazaki et al.

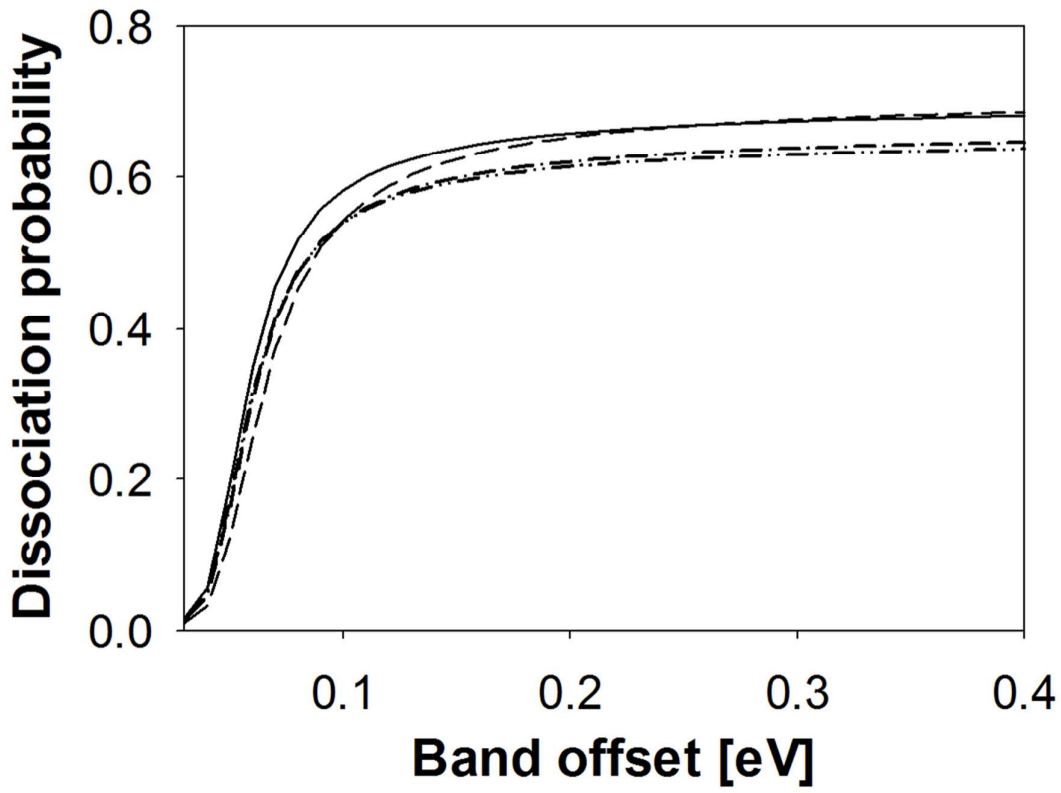

Figure 2b. T. Shimazaki et al.

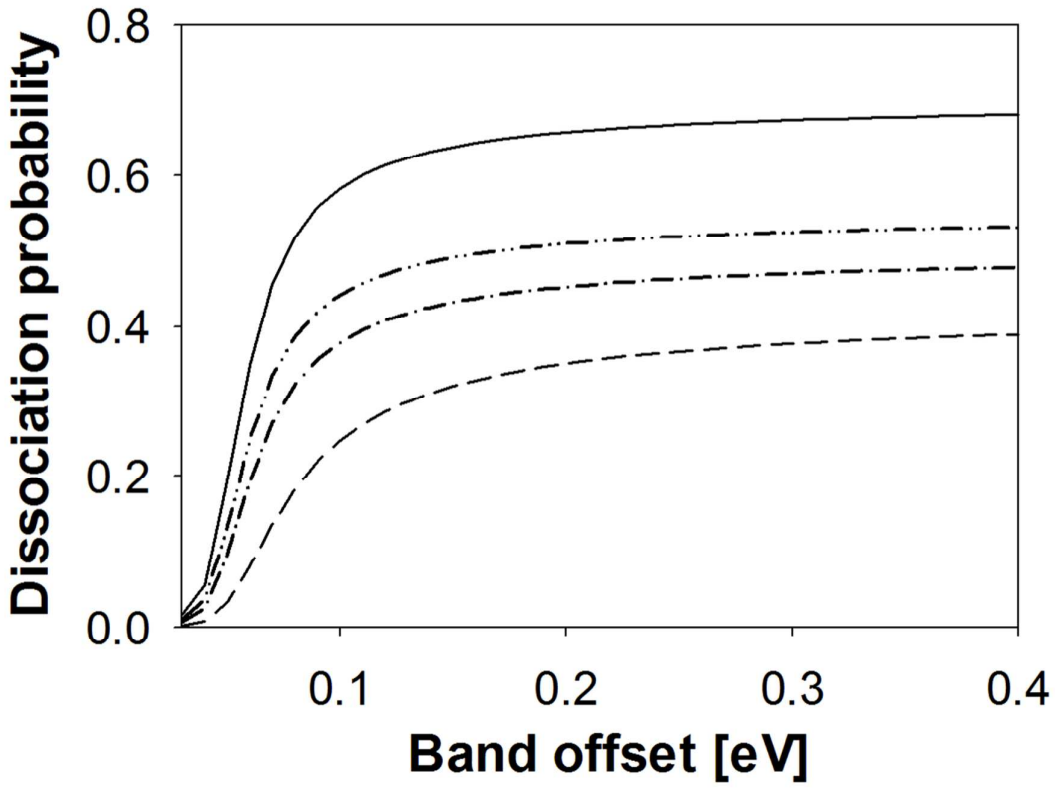

Figure 2c. T. Shimazaki et al.

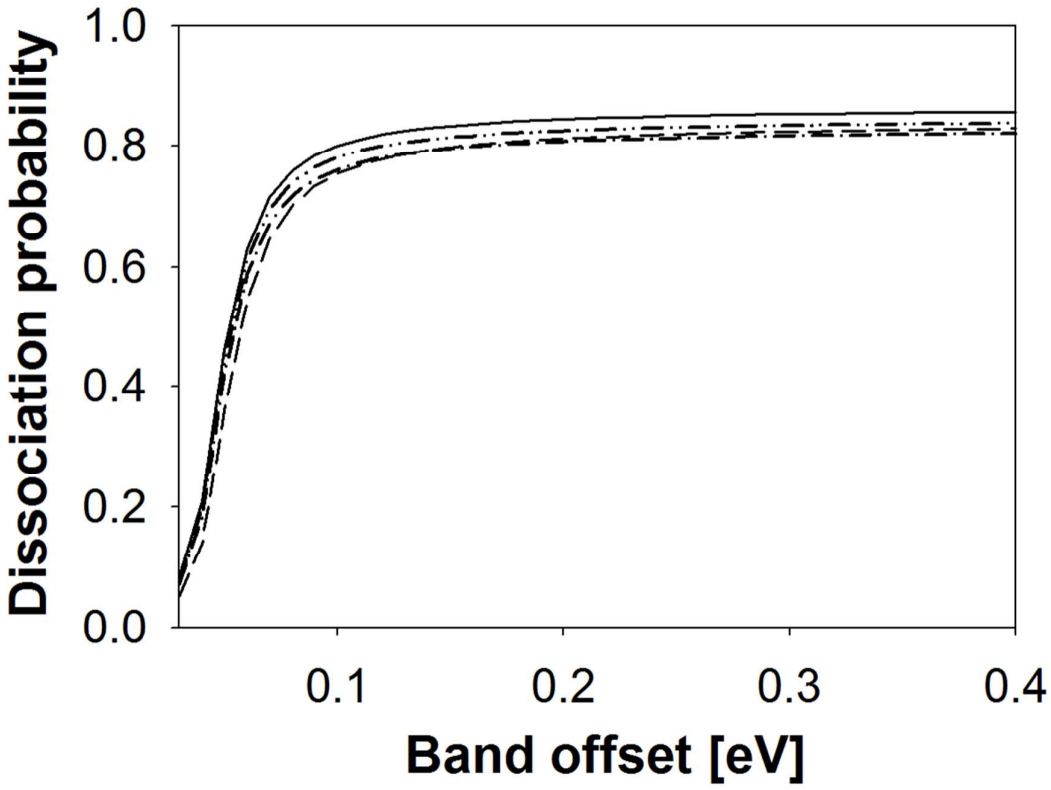

Figure 3a. T. Shimazaki et al.

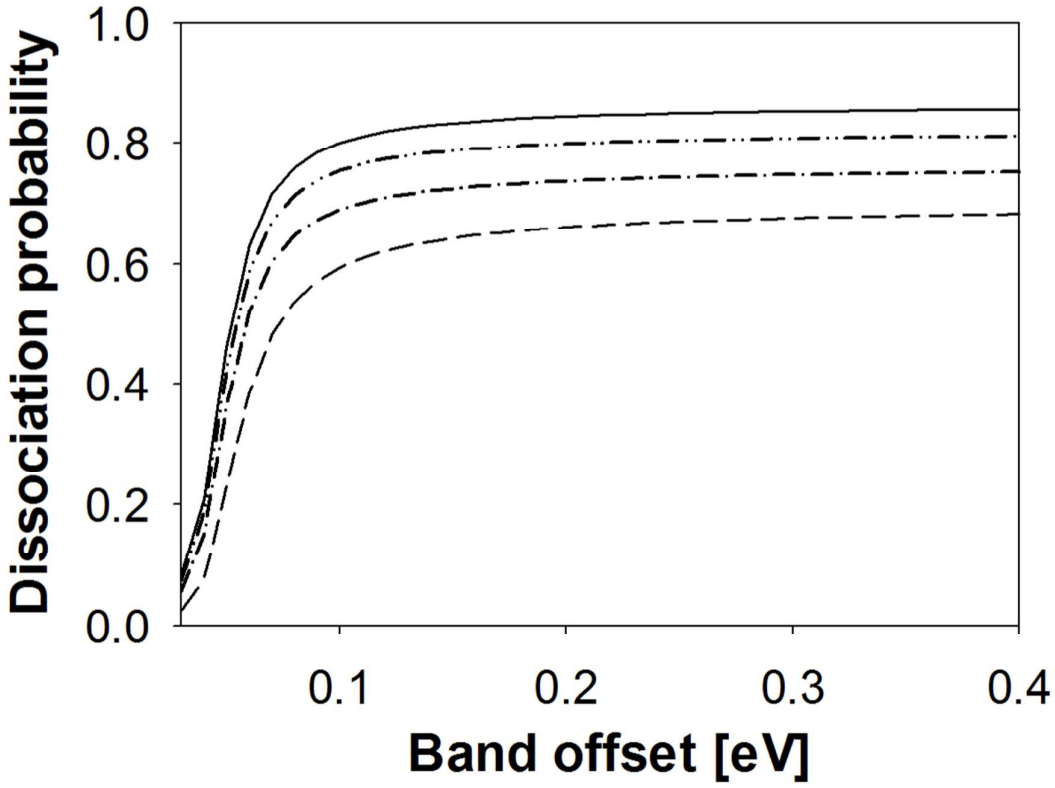

Figure 3b. T. Shimazaki et al.

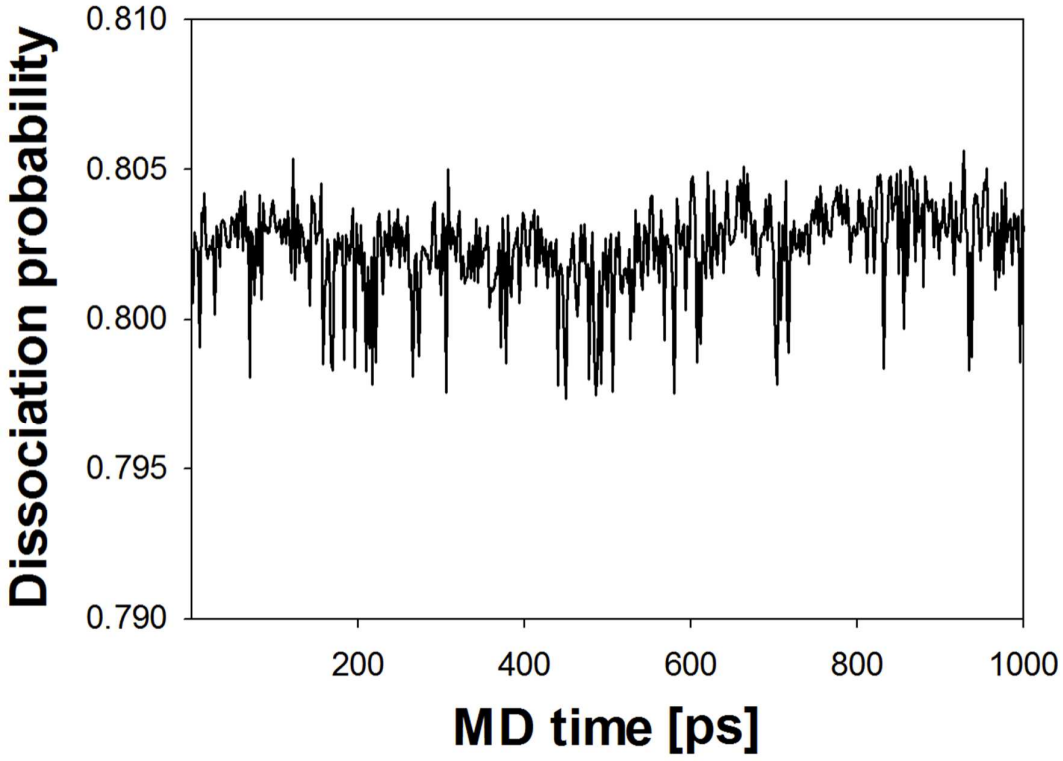

Figure 4a. T. Shimazaki et al.

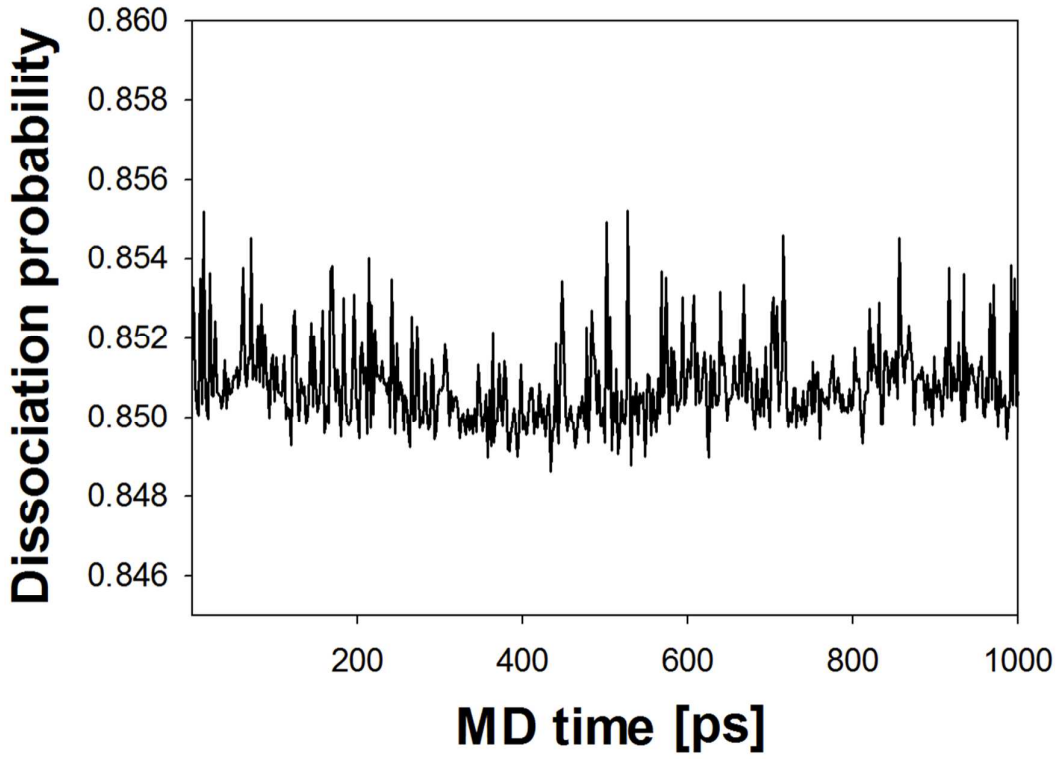

Figure 4b. T. Shimazaki et al.

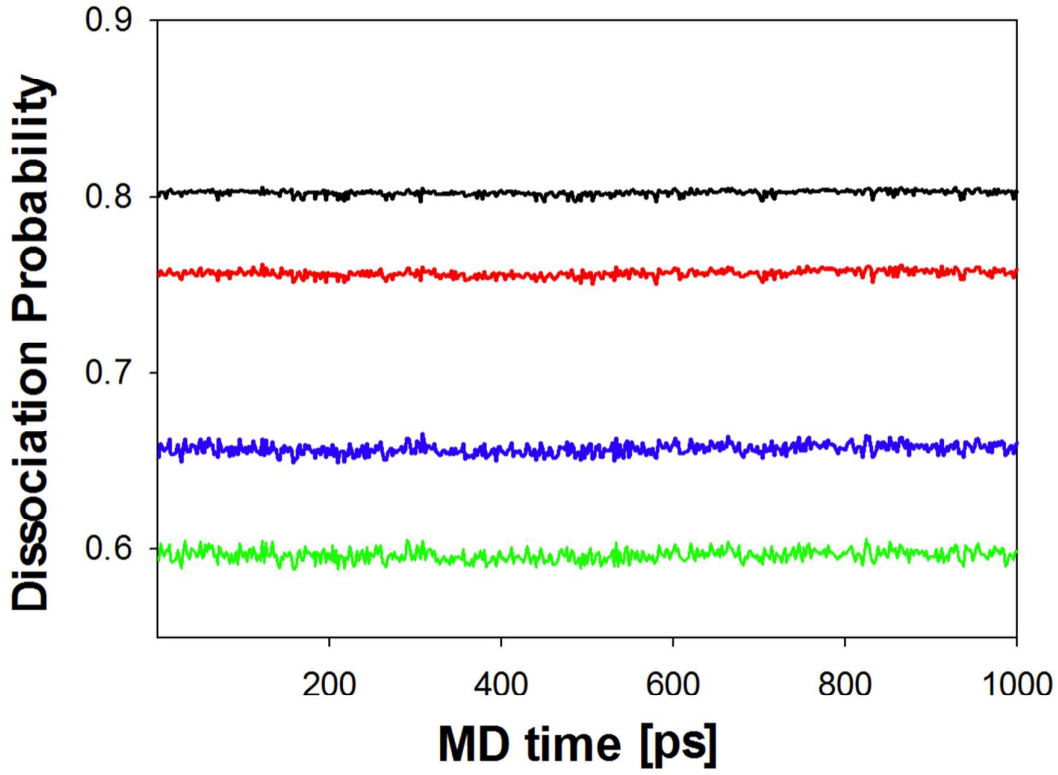

Figure 5a. T. Shimazaki et al.

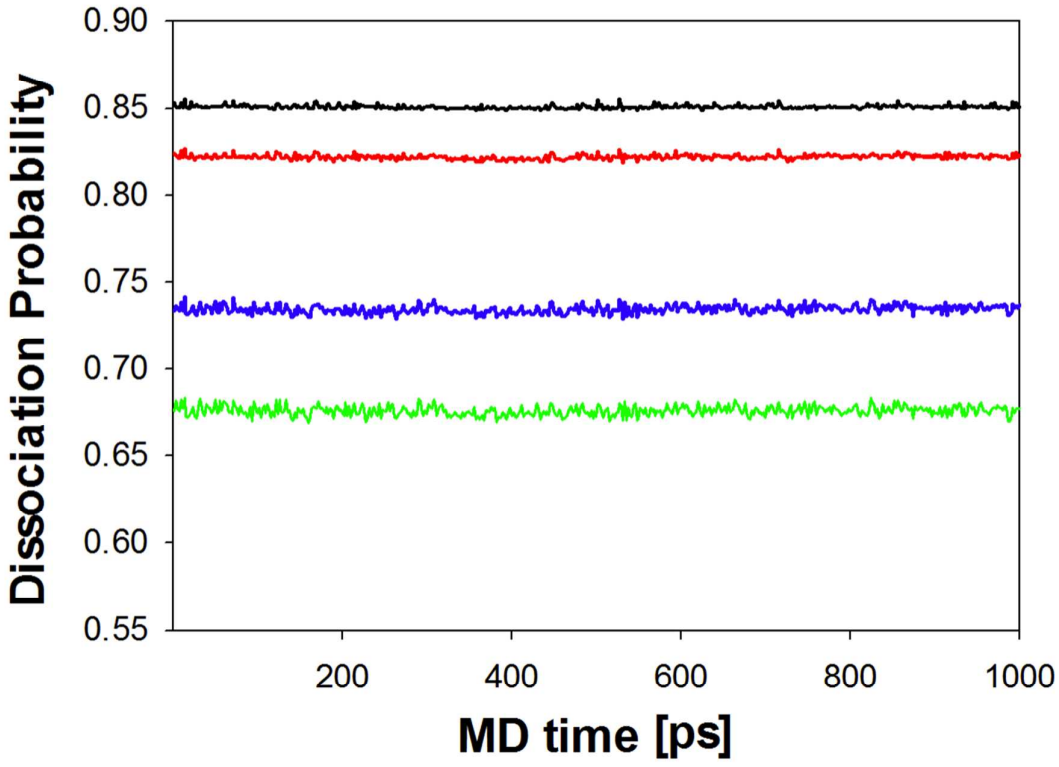

Figure 5b. T. Shimazaki et al.

References

1. T. M. Clarke and J. R. Durrant, *Chem Rev*, 2010, **110**, 6736-6767.
2. A. Liu, S. Zhao, S. B. Rim, J. Wu, M. Konemann, P. Erk and P. Peumans, *Adv Mater*, 2008, **20**, 1065-1070.
3. B. A. Gregg, *J Phys Chem Lett*, 2011, **2**, 3013-3015.
4. R. G. H. Wilke, G. K. Moghadam, N. H. Lovell, G. J. Suaning and S. Dokos, *Journal of Neural Engineering*, 2011, **8**, 123304.
5. D. Beljonne, J. Cornil, L. Muccioli, C. Zannoni, J. L. Bredas and F. Castet, *Chemistry of Materials*, 2011, **23**, 591-609.
6. D. P. McMahon, D. L. Cheung and A. Troisi, *J Phys Chem Lett*, 2011, **2**, 2737-2741.
7. W. Chen, T. Xu, F. He, W. Wang, C. Wang, J. Strzalka, Y. Liu, J. G. Wen, D. J. Miller, J. H. Chen, K. L. Hong, L. P. Yu and S. B. Darling, *Nano Lett*, 2011, **11**, 3707-3713.
8. G. Grancini, D. Polli, D. Fazzi, J. Cabanillas-Gonzalez, G. Cerullo and G. Lanzani, *J Phys Chem Lett*, 2011, **2**, 1099-1105.
9. S. R. Yost, L. P. Wang and T. Van Voorhis, *J Phys Chem C*, 2011, **115**, 14431-14436.
10. S. D. Baranovskii, M. Wiemer, A. V. Nenashev, F. Jansson and F. Gebhardt, *J Phys Chem Lett*, 2012, **3**, 1214-1221.
11. P. Peumans and S. R. Forrest, *Chemical Physics Letters*, 2004, **398**, 27-31.
12. A. C. Morteani, P. Sreearunothai, L. M. Herz, R. H. Friend and C. Silva, *Physical Review Letters*, 2004, **92**, 247402.
13. J. G. Muller, J. M. Lupton, J. Feldmann, U. Lemmer, M. C. Scharber, N. S. Sariciftci, C. J. Brabec and U. Scherf, *Physical Review B*, 2005, **72**, 195208
14. H. Ohkita, S. Cook, Y. Astuti, W. Duffy, S. Tierney, W. Zhang, M. Heeney, I. McCulloch, J. Nelson, D. D. C. Bradley and J. R. Durrant, *J Am Chem Soc*, 2008, **130**, 3030-3042.
15. M. Muntwiler, Q. Yang, W. A. Tisdale and X. Y. Zhu, *Physical Review Letters*, 2008, **101**, 196403.
16. S. D. Dimitrov, A. A. Bakulin, C. B. Nielsen, B. C. Schroeder, J. P. Du, H. Bronstein, I. McCulloch, R. H. Friend and J. R. Durrant, *J Am Chem Soc*, 2012, **134**, 18189-18192.
17. A. A. Bakulin, A. Rao, V. G. Pavelyev, P. H. M. van Loosdrecht, M. S. Pshenichnikov, D. Niedzialek, J. Cornil, D. Beljonne and R. H. Friend, *Science*, 2012, **335**, 1340-1344.
18. G. Grancini, M. Maiuri, D. Fazzi, A. Petrozza, H. J. Egelhaaf, D. Brida, G. Cerullo and G. Lanzani, *Nature Materials*, 2013, **12**, 29-33.
19. A. E. Jailaubekov, A. P. Willard, J. R. Tritsch, W. L. Chan, N. Sai, R. Gearba, L. G.

Kaake, K. J. Williams, K. Leung, P. J. Rossky and X. Y. Zhu, *Nature Materials*, 2013, **12**, 66-73.

20. H. Tamura and I. Burghardt, *J Am Chem Soc*, 2013, **135**, 16364-16367.
21. X. X. Shen, G. C. Han, D. Fan, Y. J. Xie and Y. P. Yi, *J Phys Chem C*, 2015, **119**, 11320-11326.
22. B. R. Gautam, R. Younts, W. T. Li, L. Yan, E. Danilov, E. Klump, I. Constantinou, F. So, W. You, H. Ade and K. Gundogdu, *Adv Energy Mater*, 2016, **6**, 1301032.
23. D. Fazzi, M. Barbatti and W. Thiel, *J Phys Chem Lett*, 2017, **8**, 4727-4734.
24. A. Y. Sosorev, D. Y. Godovsky and D. Y. Paraschuk, *Phys Chem Chem Phys*, 2018, **20**, 3658-3671.
25. T. Shimazaki and T. Nakajima, *Phys Chem Chem Phys*, 2015, **17**, 12538-12544.
26. T. Shimazaki and T. Nakajima, *Journal of Chemical Physics*, 2016, **144**, 234906.
27. T. Shimazaki and T. Nakajima, *Phys. Chem. Chem. Phys.*, 2016, **18**, 27554.
28. T. Shimazaki and T. Nakajima, *Phys Chem Chem Phys*, 2017, **19**, 12517-12526.
29. M. Hiramoto, H. Fujiwara and M. Yokoyama, *Applied Physics Letters*, 1991, **58**, 1062-1064.
30. M. Hiramoto, H. Fujiwara and M. Yokoyama, *Journal of Applied Physics*, 1992, **72**, 3781-3787.
31. N. S. Sariciftci, D. Braun, C. Zhang, V. I. Srdanov, A. J. Heeger, G. Stucky and F. Wudl, *Applied Physics Letters*, 1993, **62**, 585-587.
32. G. Yu, J. Gao, J. C. Hummelen, F. Wudl and A. J. Heeger, *Science*, 1995, **270**, 1789-1791.
33. E. Kawashima, M. Fujii and K. Yamashita, *Phys Chem Chem Phys*, 2016, **18**, 26456-26465.
34. R. Alessandri, J. J. Uusitalo, A. H. de Vries, R. W. A. Havenith and S. J. Marrink, *J Am Chem Soc*, 2017, **139**, 3697-3705.
35. R. C. Masters, A. J. Pearson, T. S. Glen, F. C. Sasam, L. T. Li, M. Dapor, A. M. Donald, D. G. Lidzey and C. Rodenburg, *Nat Commun*, 2015, **6**, 6928.
36. A. Miller and E. Abrahams, *Physical Review*, 1960, **120**, 745-755.
37. A. V. Nenashev, S. D. Baranovskii, M. Wiemer, F. Jansson, R. Osterbacka, A. V. Dvurechenskii and F. Gebhard, *Physical Review B*, 2011, **84**, 035210.
38. V. I. Arkhipov, E. V. Emelianova and H. Bassler, *Physical Review Letters*, 1999, **82**, 1321-1324.
39. V. I. Arkhipov, E. V. Emelianova, S. Barth and H. Bassler, *Physical Review B*, 2000, **61**, 8207-8214.
40. L. Onsager, *Journal of Chemical Physics*, 1934, **2**, 599-615.

41. J. Frenkel, *Physical Review*, 1938, **54**, 647-648.
42. K. M. Hong and J. Noolandi, *Surface Science*, 1978, **75**, 561-576.
43. H. Sano and M. Tachiya, *Journal of Chemical Physics*, 1979, **71**, 1276-1282.
44. M. Hilczer and M. Tachiya, *J Phys Chem C*, 2010, **114**, 6808-6813.
45. O. Rubel, S. D. Baranovskii, W. Stolz and F. Gebhard, *Physical Review Letters*, 2008, **100**, 196602.
46. W. L. Jorgensen, D. S. Maxwell and J. TiradoRives, *J Am Chem Soc*, 1996, **118**, 11225-11236.
47. D. L. Cheung and A. Troisi, *J Phys Chem C*, 2010, **114**, 20479-20488.
48. M. Casalegno, S. Zanardi, F. Frigerio, R. Po, C. Carbonera, G. Marra, T. Nicolini, G. Raos and S. V. Meille, *Chem Commun*, 2013, **49**, 4525-4527.
49. *LAMMPS program package, http://lammps.sandia.gov (accessed Oct. 4, 2017).*
50. S. Plimpton, *J Comput Phys*, 1995, **117**, 1-19.
51. F. Gajdos, H. Oberhofer, M. Dupuis and J. Blumberger, *J Phys Chem Lett*, 2013, **4**, 1012-1017.
52. J. Tsutsumi, H. Matsuzaki, N. Kanai, T. Yamada and T. Hasegawa, *J Phys Chem C*, 2013, **117**, 16769-16773.
53. I. G. Scheblykin, A. Yartsev, T. Pullerits, V. Gulbinas and V. Sundstrom, *J Phys Chem B*, 2007, **111**, 6303-6321.
54. K. Chen, A. J. Barker, M. E. Reish, K. C. Gordon and J. M. Hodgkiss, *J Am Chem Soc*, 2013, **135**, 18502-18512.
55. J. M. Szarko, B. S. Rolczynski, S. J. Lou, T. Xu, J. Strzalka, T. J. Marks, L. P. Yu and L. X. Chen, *Advanced Functional Materials*, 2014, **24**, 10-26.
56. K. Kawashima, Y. Tamai, H. Ohkita, I. Osaka and K. Takimiya, *Nat Commun*, 2015, **6**, 1.
57. J. Rivnay, S. C. B. Mannsfeld, C. E. Miller, A. Salleo and M. F. Toney, *Chem Rev*, 2012, **112**, 5488-5519.
58. Y. Huang, E. J. Kramer, A. J. Heeger and G. C. Bazan, *Chem Rev*, 2014, **114**, 7006-7043.
59. P. K. Watkins, A. B. Walker and G. L. B. Verschoor, *Nano Lett*, 2005, **5**, 1814-1818.
60. B. P. Lyons, N. Clarke and C. Groves, *Energ Environ Sci*, 2012, **5**, 7657-7663.
61. C. K. Lee and C. W. Pao, *J Phys Chem C*, 2014, **118**, 11224-11233.
62. C. M. Du, Y. J. Ji, J. W. Xue, T. J. Hou, J. X. Tang, S. T. Lee and Y. Y. Li, *Sci Rep-Uk*, 2015, **5**, 16854.
63. C. Groves, *Rep. Prog. Phys.*, 2016, **80**, 026502.
64. T. M. Burke and M. D. McGehee, *Adv Mater*, 2014, **26**, 1923-1928.

65. Q. Wu, *J Phys Chem B*, 2015, **119**, 7321-7327.
66. M. Wiemer, M. Koch, U. Lemmer, A. B. Pevtsov and S. D. Baranovskii, *Organic Electronics*, 2014, **15**, 2461-2467.
67. B. C. Thompson and J. M. J. Frechet, *Angewandte Chemie-International Edition*, 2008, **47**, 58-77.
68. J. M. Guo, H. Ohkita, H. Benten and S. Ito, *J Am Chem Soc*, 2010, **132**, 6154-6164.
69. O. G. Reid, R. D. Pensack, Y. Song, G. D. Scholes and G. Rumbles, *Chemistry of Materials*, 2014, **26**, 561-575.
70. Y. Tamai, K. Tsuda, H. Ohkita, H. Benten and S. Ito, *Phys Chem Chem Phys*, 2014, **16**, 20338-20346.
71. M. Hiramoto, T. Yamaga, M. Danno, K. Suemori, Y. Matsumura and M. Yokoyama, *Applied Physics Letters*, 2006, **88**, 213105.

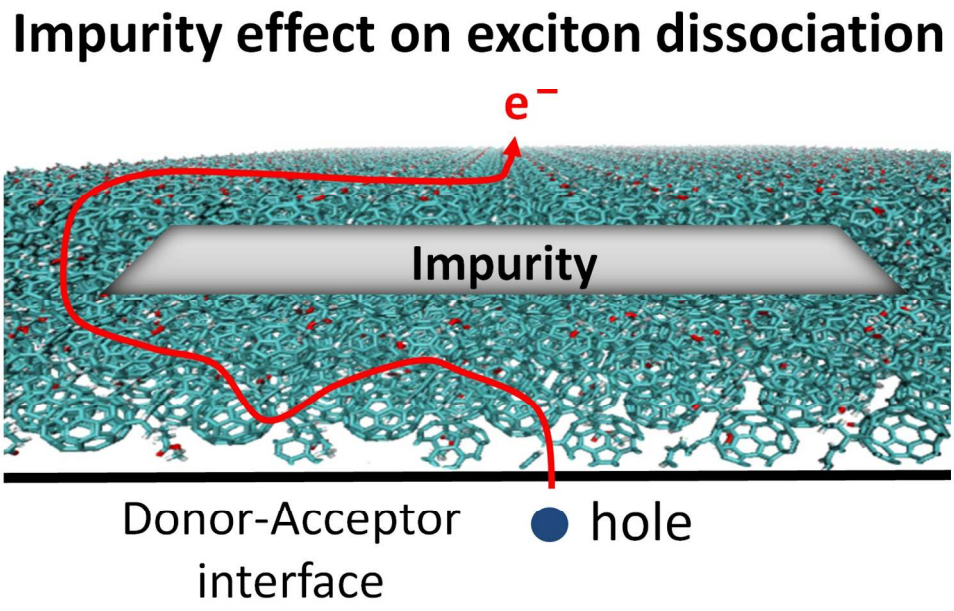

301x190mm (144 x 144 DPI)